Ferrimagnetism and metal–insulator transition in an organic polymer chain*

Ding Lin-Jie(丁林杰)†, Zhong Yuan(钟 园), and Fan Shuai-Wei(樊帅伟)

Department of Physics, China Three Gorges University, Yichang 443002, *China*

(Received 29 April 2013; revised manuscript received 8 June 2013; published online 10 December 2013)

The ferrimagnetism and quantum phase transition of a bipartite lozenge periodic Anderson-like organic polymer, in which the localized f electrons hybridize with the odd site conduction orbitals, are investigated by means of Green's function theory. The ground state turns out to be gapless ferrimagnetism. At a finite temperature, the ferrimagnetic-to-paramagnetic phase transition takes place. The Kondo screenings and Ruderman–Kittel–Kasuya–Yosida (RKKY) interaction can reduce and increase the transition temperature, respectively. Two Kondo screenings compete with each other, giving rise to the localized f electron spin screened antiferromagnetically. Accordingly, in a magnetic field, all spins are aligned along the chain easily, which is associated with metal–insulator transition. Furthermore, in a temperature-field plane, we reveal the gapless and spin polarized phases, which are characterized by susceptibility and specific heat, and whose behaviours are determined by the competition between the up-spin and down-spin hole excitations.

Keywords: ferrimagnetism, quantum phase transition, organic polymer

PACS: 75.50.Gg, 73.43.Nq, 75.40.Cx **DOI:** 10.1088/1674-1056/23/2/027502

1. Introduction

The magnetisms and quantum criticalities of low-dimensional organic quantum magnets have attracted much attention both experimentally and theoretically in recent years.[1–24] Many quasi-one-dimensional (1D) organic ferromagnets have been reported, such as poly-BIPO,[1] p-NPNN,[2] and 2-benzimidazolyl nitronyl nitroxide (2-BIMNN).[20] Particularly intriguing are the conjugated organic polymers with electronic correlations.[3–14,19,21–23] Heeger *et al.*,[26–28] who first discovered the conducting organic polymers, have conducted intensive studies, paving a new way to realize various functions in molecular-electronic or spintronic devices with organic polymers or oligomers like transistors[29] or spin-valves.[30] Meanwhile, the design of organic polymers to realize ferromagnetism is becoming increasingly realistic.[19] Ovchinnikov[31] first proposed an idea to obtain organic ferromagnets, which is the synthesis of alternate hydrocarbon with a high-spin ground state, where the π-electrons along the main zigzag chain were considered to be itinerant, while the unpaired electrons on the side radicals were regarded as being delocalized or localized (see Fig. 1(a)). Subsequently, the Su–Schrieffer–Heeger (SSH) and Hubbard models[3–8,21] were proposed to describe this quasi-1D conjugated organic polymer, considered as a delocalized π-electron system, where the orbitals of successive carbon atoms overlap, giving rise to charge mobility along the backbone of the polymer chain. Besides this, Wang[14] proposed a periodic Anderson-like model to describe this conjugated organic polymer, whose ground state properties were studied using an exact diagonalization technique. Within this model, the conduction electrons with uncorrelated orbitals which reside in the main zigzag chain form a conduction sea, while a correlated localized f orbital is located at the side radical R (as illustrated in Fig. 1(a)). In this structure, since the f electrons are strongly localized, while the conduction electrons form a conduction sea distributed throughout the system, which presents a Fermi liquid coupling with localized spins, two interactions compete between each other.[32–35] One interaction is the Kondo coupling, which happens as the spin of the localized f electron is screened by the conduction orbital $(l,2)$, favoring a nonmagnetic singlet state; the other is the superexchange, i.e. the indirect ferromagnetic Ruderman–Kittel–Kasuya–Yosida (RKKY) interaction of the two contiguous localized spins mediated by a conduction sea, which tends to stabilize a magnetically ordered phase. As is well known, the Kondo coupling $J_{\rm K} \sim V^2/U$,[36] implies that the behaviour of the system is controlled by two parameters: the hybridization V and the Hubbard repulsion U. Thus, the interplay between Coulomb interaction and hybridization accounts for the competition between Kondo coupling and RKKY interaction. In addition, another interesting structure for the organic polymer is the bipartite lozenge lattice shown in Fig. 1(b), which was described by a Hubbard model, manifesting a ferrimagnetic insulating ground state.[3,4,9,11] However, in contrast to Fig. 1(a), the uncorrelated conduction orbitals are still located at the zigzag chain, while the localized f orbital is located at the side radi-

*Project supported by the National Natural Science Foundation of China (Grant Nos. 11204157 and 11174179), the China Three Gorges University Project (Grant No. KJ2011B068), and the Yichang City Project, China (Grant No. A201230229).

†Corresponding author. E-mail: dinglinjie82@126.com

© 2014 Chinese Physical Society and IOP Publishing Ltd

cal R hybridized with the odd site conduction orbitals. This results in a bipartite lozenge chain, which can also be described as a periodic Anderson-like model.

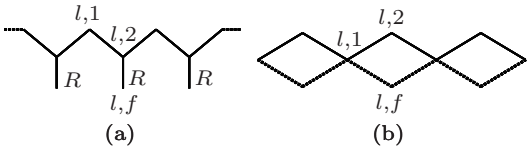


Fig. 1. (a) A quasi-one-dimensional organic polymer chain and (b) a bipartite lozenge chain.

In this bipartite lozenge periodic Anderson-like organic polymer, at half filling, though the ground state lies in the gapless ferrimagnetic phase, it is neither metallic nor insulating. Different from Fig. 1(a), two Kondo screenings compete between each other, resulting in the localized f electron spin screened antiferromagnetically. Thus, as the magnetic field is turned on, it will make all spins align along the chain easily, together with a metal–insulator transition. At a finite temperature, phase crossover behaviors are expected. Accordingly, we shall explore the magnetic properties and quantum phase transition (QPT)[37–39] for this periodic Anderson-like organic polymer using Green's function theory in an external magnetic field. In the forthcoming section, we will present the Hamiltonian model and give an outline of the Green's function method. In Section 3, the energy bands, the magnetization, the susceptibility, and the specific heat will be calculated; the temperature- and field-induced phase diagrams will be explored; and the hole excitations, which are closely related to the thermodynamic behaviors, will also be discussed. Finally, we draw a conclusion in Section 4.

2. Model Hamiltonian and method

The Hamiltonian for the bipartite lozenge periodic Anderson-like polymer chain illustrated in Fig. 1(b) in an external magnetic field reads

$$\begin{aligned} H &= -t\sum_{l,\sigma}\left(c^{\dagger}_{l,1,\sigma}c_{l,2,\sigma}+c^{\dagger}_{l,2,\sigma}c_{l+1,1,\sigma}+\text{h.c}\right) \\ &\quad +\varepsilon_f\sum_{l,\sigma}c^{\dagger}_{l,f,\sigma}c_{l,f,\sigma}+U\sum_{l}n_{l,f,\uparrow}n_{l,f,\downarrow} \\ &\quad +\sum_{l,\sigma}V\left(c^{\dagger}_{l,1,\sigma}c_{l,f,\sigma}+c^{\dagger}_{l+1,1,\sigma}c_{l,f,\sigma}+\text{h.c}\right) \\ &\quad -\frac{h}{2}\sum_{l}\sum_{\eta=1,2,f}\left(n_{l,\eta,\uparrow}-n_{l,\eta,\downarrow}\right), \end{aligned} \tag{1}$$

where t is the hopping integral between the nearest-neighbouring conduction orbitals; $c^{\dagger}_{l,\eta,\sigma}$ and $c_{l,\eta,\sigma}$ $(\eta=1,2,f)$ denote the creation and annihilation operators with spin $\sigma=\uparrow,\downarrow$ for the conduction and localized f electrons, respectively; $n^{\eta}_{l,\sigma}=c^{\dagger}_{l,\eta,\sigma}c_{l,\eta,\sigma}$ is the number operator; ε_f is the bare energy of the localized f orbital; U is the f orbital electron–electron Coulomb repulsion; V is the hybridization, denoting the f electrons screened by conduction orbital $(l,\ 1)$; $h=g\mu_{\text{B}}B$ is the reduced magnetic field (Zeeman energy) with g being the Landé g factor, μ_{B} the Bohr magneton, and B the magnetic field.

Now, we employ the equations of motion to calculate the retarded Green's function[17,23,40–42] for the electrons, which is defined as

$$\begin{aligned} G^{\sigma}_{ij}(t_1-t_2) &= \langle\langle c_{i,\sigma}(t_1);c^{\dagger}_{j,\sigma}(t_2)\rangle\rangle \\ &= -\text{i}\,\theta(t_1-t_2)\left\langle c_{i,\sigma}c^{\dagger}_{j,\sigma}+c^{\dagger}_{j,\sigma}c_{i,\sigma}\right\rangle, \end{aligned} \tag{2}$$

where the subscripts i and j denote the lattice sites. After the time Fourier transformation, the Green's function is put into the equation of motion,

$$\begin{aligned} &\omega\langle\langle c_{i,\sigma};c^{\dagger}_{j,\sigma}\rangle\rangle \\ &=\left\langle\left[c_{i,\sigma},c^{\dagger}_{j,\sigma}\right]_{+}\right\rangle+\langle\langle[c_{i,\sigma},H];c^{\dagger}_{j,\sigma}\rangle\rangle. \end{aligned} \tag{3}$$

By performing the equation of motion analogous to Eq. (3) for the high-order Green's function $\langle\langle[c_{i,\sigma},H];c^{\dagger}_{j,\sigma}\rangle\rangle$, the higher-order Green's function will appear on the right side, resulting in an infinite set of coupled equations. In terms of Wick's theorem, we adopt the decoupling scheme for the four-operator Green's functions,[42]

$$\langle\langle A^{\dagger}BC;D^{\dagger}\rangle\rangle\approx\langle A^{\dagger}B\rangle\langle\langle C;D^{\dagger}\rangle\rangle-\langle A^{\dagger}C\rangle\langle\langle B;D^{\dagger}\rangle\rangle. \tag{4}$$

Herein, it is noted that the Green's functions are diagonal in spin space $G^{\sigma\sigma'}_{ij}=G^{\sigma}_{ij}\delta_{\sigma\sigma'}$.

For further Fourier transformation into k-space, the Green's function reads

$$G^{\sigma}_{ij}=\frac{1}{N}\sum_{k}g^{\sigma}(k,\omega)\,\text{e}^{\text{i}k\cdot(i-j)}. \tag{5}$$

The integral of the wavevector k extends over the first Brillouin zone. Accordingly, the momentum space Green's function $g^{\sigma}(k,\omega)$ behaves as a function of a wave vector k and the elementary excitation spectrum $\omega=\omega(k)$.

Associated with the standard spectral theorem, the correlation function of the product of the electron operators can be expressed as

$$\begin{aligned} &\left\langle c^{\dagger}_{j,\mu,\sigma}c_{i,\nu,\sigma}\right\rangle \\ &=\frac{\text{i}}{2\pi N}\sum_{k}\text{e}^{\text{i}k\cdot(i-j)} \\ &\quad\times\int\frac{g^{\sigma}_{\mu\nu}\left(k,\omega+\text{i}0^{\dagger}\right)-g^{\sigma}_{\mu\nu}\left(k,\omega-\text{i}0^{\dagger}\right)}{\text{e}^{\beta\omega}+1}\text{d}\omega, \end{aligned} \tag{6}$$

where $\beta=1/k_{\text{B}}T$, with k_{B} being the Boltzman's constant, and T the absolute temperature.

The spin density (sublattice magnetization) at one site is defined as

$$\left\langle S^{z}_{l,\eta}\right\rangle=\frac{1}{2}\left(\left\langle n^{\eta}_{l,\uparrow}\right\rangle-\left\langle n^{\eta}_{l,\downarrow}\right\rangle\right),\quad(\eta=1,2,f). \tag{7}$$

Then the average magnetization of the unit cell and the magnetic susceptibility are obtained as follows:

$$M = \frac{1}{N}\sum_{l}\left(\left\langle S^{z}_{l,1}\right\rangle + \left\langle S^{z}_{l,2}\right\rangle + \left\langle S^{z}_{l,f}\right\rangle\right), \quad \chi = \frac{\partial M}{\partial h}. \tag{8}$$

Likewise, the specific heat can be attained as

$$C_{\mathrm{V}} = \frac{\mathrm{d}\langle H\rangle}{\mathrm{d}T}. \tag{9}$$

Accordingly, the above equations can be solved self-consistently.[23] In calculation, an initial state, composed of a set of electron numbers and a spin density of f orbital, is put into the equations to produce resulting values. The iteration goes on until convergence is reached.

3. Results and discussion

We first discuss the sublattice magnetization (spin density) and the temperature-induced phase diagrams for the bipartite lozenge periodic Anderson-like chain at half filling. In what follows, all parameters are scaled by the hopping integral t, which is set as a unit. For the symmetrical case $U+2\varepsilon_f = 0$, there is no charge fluctuation, and the ground state always lies in a ferrimagnetic phase which is clearly manifested in the insets of Figs. 2(a) and 2(c), where the magnetization per unit cell $M = 0.5 = M_{\mathrm{s}}/3$ ($M_{\mathrm{s}} = 1.5$ is the saturation magnetization). On the one hand, for $U = 2.0$, it is evident that the sublattice magnetizations $\langle S^{z}_{2}\rangle, \langle S^{z}_{f}\rangle > 0$, and $\langle S^{z}_{1}\rangle < 0$, indicating antiferromagnetic correlations between conduction orbitals, and also between localized f orbital and conduction orbital $(l,1)$ as shown in the inset of Fig. 2(a). Although $\langle S^{z}_{1}\rangle < 0$, its absolute value is close to zero, implying the serious double occupation on the conduction orbital (l, 1). Nevertheless, the sublattice magnetization $\langle S^{z}_{2}\rangle$ increases monotonically with the increasing of hybridization V, whereas it is opposite to $\langle S^{z}_{f}\rangle$, implying that the spin density mainly transfers from the localized f orbital to the conduction orbital (l, 2) through the conduction orbital (l, 1). Figure 2(a) manifests the temperature dependences of sublattice magnetization $\langle S^{z}_{\alpha}\rangle$ ($\alpha = 1,2,f$) for different hybridizations. In weak hybridization, the f orbital is nearly singly occupied and highly localized, which mainly contributes to the ferrimagnetism, while a large double occupation is located on the conduction orbitals, implying that the paramagnetism-like (disorder) behavior takes place in the main zigzag chain. In this case, the indirect RKKY interaction predominates. With the increasing of V, the transition temperature T_{C} ($T \to T_{\mathrm{C}}$, $M \to 0$) declines because the Kondo screening becomes more and more dominant and the chain shows ferromagnetic correlation between adjacent conduction orbitals (l, 2) and ($l+1$, 2) gradually, of which the magnetic moment becomes frangible with respect to temperature. As V is very large, the conduction orbital (l, 2) is nearly singly occupied while the f orbital is seriously doubly occupied, giving rise to the very weak spin correlation between two f orbitals (indirect RKKY interaction). Thus, we construct the T–V phase diagram as shown in Fig. 2(b), from which it is found that the transition temperature decreases monotonically with the increasing of V, revealing the enhancement of Kondo screenings against ferrimagnetic order. On the other hand, for $V = 1.0$, at zero temperature, $\langle S^{z}_{2}\rangle$ and $\langle S^{z}_{f}\rangle$ decrease and increase monotonically with the increasing of U (see the inset of Fig. 2(c)), respectively, suggesting that the spin density mainly transfers from the conduction orbitals to the localized f orbital. Figure 2(c) manifests the plots of sublattice magnetization $\langle S^{z}_{\alpha}\rangle$ ($\alpha = 1,2,f$) versus temperature for different U values. With the increasing of U, the transition temperature ascends and the spin density transfers to the localized f orbital gradually, resulting in a singly occupied f orbital and the enhancement of RKKY interaction favouring a ferrimagnetic state. The corresponding T–U phase diagram is plotted in Fig. 2(d). It is clearly seen that with the increasing of U, the transition temperature ascends, suggesting that the ferrimagnetism is stabilized by the Hubbard repulsion, which is consistent with the result of the ground state obtained by Wang.[9]

In order to present the natures of different magnetic and conduction states, we plot the energy bands in Fig. 3, where there are three up-spin and three down-spin bands. The Fermi level is located at $E_{\mathrm{F}} = 0$, below which two up-spin and one down-spin bands are completely occupied. Therefore, the ground state is ferrimagnetic and possesses the net spin $S = 0.5$ per unit cell, which is also demonstrated in the insets of Fig. 2. In weak hybridization, the flat parts of the bands far below Fermi level are almost occupied by the f electrons (see Fig. 3(a) for $V = 0.1$), which is hardly excited at low temperature and mainly contributes to the ferrimagnetism, reflecting the large single occupation on the localized f orbital. As V ascends, the flat band broadens and approaches Fermi level gradually as shown in Fig. 3(b) for $V = 1.0$. In this case, the single occupation on conduction orbital (l, 2) is enhanced. In fact, both the conduction orbitals and localized f orbital are partially doubly occupied. In the large-V limit, the split of the energy band with respect to spin becomes much smaller and the intermediate energy bandwidth becomes narrower, as shown in Fig. 3(c) for $V = 2.0$ clearly. Here, the conduction orbital (l, 2) is almost singly occupied and the nearly double occupation is located on the f orbital. Hence, the conduction orbital (l, 2) mainly contributes to the ferrimagnetism, which is also demonstrated in the inset of Fig. 2(a). It should be pointed out that the intermediate up-spin band is very close to Fermi level, which is excited easily at low temperature. That is why the transition temperature increases with U ascending, but decreases with V ascending. On the whole, the system is gapless, but it is neither metallic nor insulating.

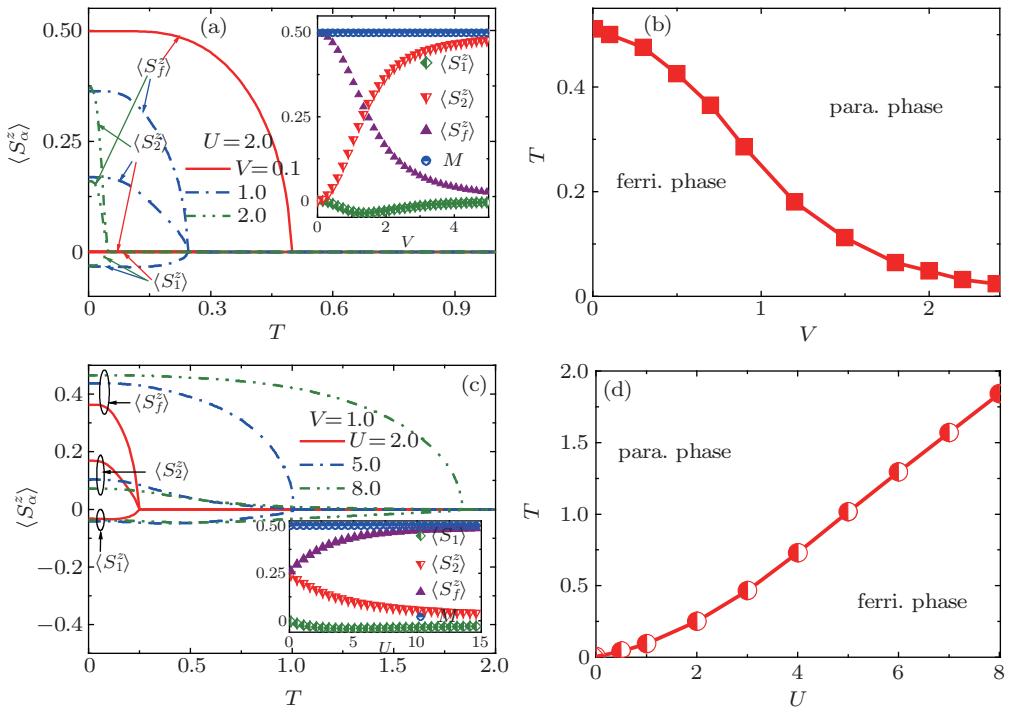


Fig. 2. (color online) (a) Variations of sublattice magnetization (spin density) with temperature for different V values with $U = 2.0$; the inset shows the curves of sublattice magnetization versus V at zero temperature. (b) The T–V phase diagram, wherein a ferrimagnetic (ferri.) phase transits into paramagnetism (para.) phase. (c) Variations of sublattice magnetization with temperatures for different U values with $V = 1.0$; the inset displays the curves of sublattice magnetization versus U at zero temperature. The corresponding T–U phase diagram is shown in panel (d).

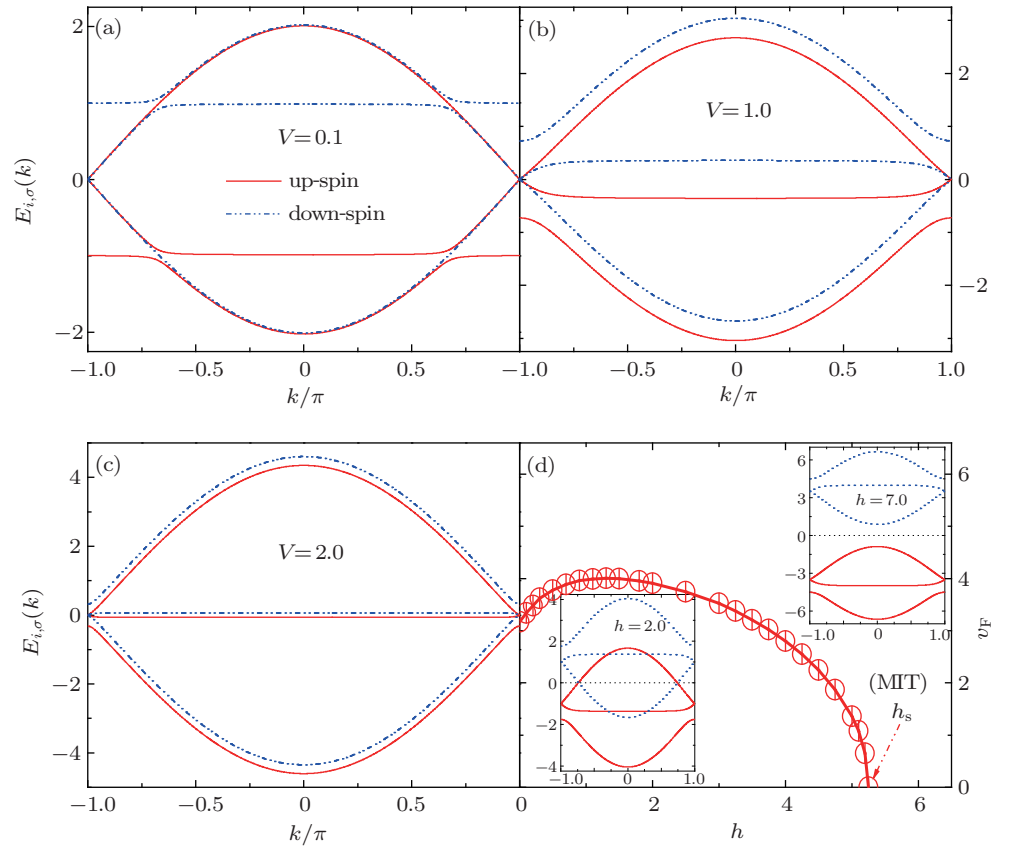


Fig. 3. (color online) Energy bands $E_{i,\sigma}(k)$ for $V = 0.1$ in panels (a), $V = 1.0$ in panels (b), and $V = 2.0$ in panels (c) with $U = 2.0$. (d) The Fermi velocity v_F as a function of h, at h_s the Metal–Insulator–Transition (MIT) occurs, the insets show the energy bands under different phases.

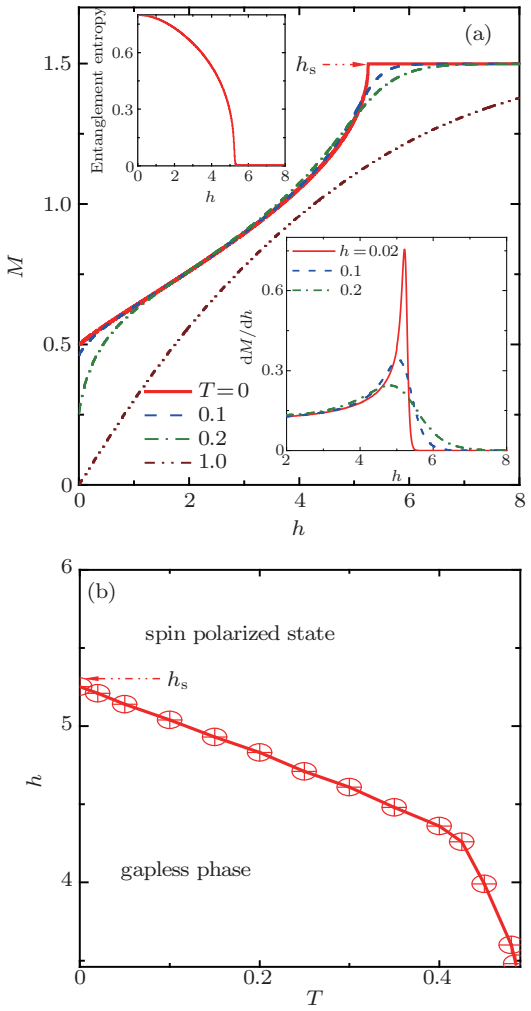


Fig. 4. (color online) (a) Variations of magnetization with h for different temperatures; the upper inset shows the entanglement entropy against h at zero temperature; the lower inset exhibits the curves of dM/dh versus h for different temperatures. (b) h–T phase diagram: the phase boundary between the gapless regime and the spin polarized state, results from (h, T) values corresponding to the maximum of dM/dh as shown in the lower inset of panel (a).

As the magnetic field is turned on, a metal–insulator transition will occur. Recalling Fig. 2, for $V = 1.0$, the spins of partial electrons on the localized f orbital are screened by contiguous conduction orbitals $(l, 1)$ and $(l+1, 1)$, giving rise to two Kondo screenings which compete with each other. Accordingly, the localized f electron spin is screened antiferromagnetically. Thus, in a magnetic field, it will make all spins align along the chain rapidly. Figure 4(a) shows the magnetization curves for different temperatures, and at zero temperature, it clearly shows a critical field h_s (labeled in the figure), suggesting the QPT may occur. As is well known, the single-site (localized f orbital) entanglement entropy $E_v = -z\log_2 z - u^+\log_2 u^+ - u^-\log_2 u^- - w\log_2 w$,[38,43,44] where $w = \langle n_{f\uparrow} n_{f\downarrow}\rangle$, $u^+ = \langle n_{f\uparrow}\rangle - w$, $u^- = \langle n_{f\downarrow}\rangle - w$, and $z = 1 - \langle n_{f\uparrow}\rangle - \langle n_{f\downarrow}\rangle + w$, is a good indicator of QPT, as shown in the upper inset of Fig. 4(a), wherein E_v vanishes as $h > h_s$, which corresponds to the fully polarized state (singly occupied state). In fact, the magnetic field acts as a Fermi level or chemical potential. As it increases, the down-spin bands are lifted while the up-spin ones are lowered, leading to the intermediate up-spin and down-spin bands traversing the Fermi level (see the lower inset of Fig. 3(d)). For the field beyond h_s, the system shows ferromagnetism and all up-spin bands are below the Fermi level while all down-spin ones are above it (see the upper inset of Fig. 3(d)) with an energy gap opened up. The critical field h_s manifests the phase transition from metallic state to ferromagnetic insulator, which is demonstrated by the plot of Fermi velocity versus magnetic field[45,46] as shown in Fig. 3(d). At a finite temperature, the critical field is rounded and the M–h curve becomes smooth. The peak of dM/dh moves towards low field with temperature increasing (see the lower inset), which can depict the crossover of two phases.[47,48] Accordingly, a (T, h) phase diagram can be constructed from the shifts of the peak of dM/dh as shown in Fig. 4(b). Strictly speaking, only for $T = 0$, QPT happens at h_s, which is induced solely by quantum fluctuations, whereas at a finite temperature only a crossover takes place. It can be clearly seen that a crossover line separates the gapless phase from the spin polarized state. The magnetic susceptibility and specific heat will be calculated to characterize with corresponding phases.

At low temperatures, the magnetic susceptibility reflects the gapless or gapped low-lying excitations under different fields. As the intermediate energy bands are located near the Fermi level, the low-lying excitations with minus energies are regarded as being of hole type. Thus, at low temperature, the susceptibility is determined by the competition between the down-spin and up-spin hole excitations near the Fermi level. In a weak field, the susceptibility displays a single peak, and decays to a finite value as $T \to 0$, indicating the gapless behavior as shown in Fig. 5(a). From the lower inset of Fig. 3(d), it follows that the density of the state of up-spin holes is larger than that of the down-spin ones near the Fermi level, yielding more excited up-spin holes and thus a decrease in the magnitude of the peak of susceptibility, together with the peak of susceptibility shifting towards the high temperature side. Nevertheless, when the temperature is high enough, the susceptibilities coincide under different fields, indicating the paramagnetic behavior by which the thermal fluctuations predominate. By increasing h further, a double-peak structure appears, which becomes clearer and clearer as h approaches h_s (see the inset). The first peak shifts towards the lower temperature side with its maximum ascending due to the fact that the critical fluctuation and the down-spin hole excitations become more and more dominant, and that the flat band (up-spin) is pushed down deeply to the Fermi sea. At h_s, the susceptibility diverges with the decrease of temperature, demonstrating QPT. As h goes beyond h_s but still nearby, a double-peak structure emerges again. The first peak moves towards the high temperature side as its amplitude is suppressed, because the small

gap is washed out by thermal fluctuations and only the up-spin holes are excited. However, for sufficiently high fields, the system lies in the fully polarized ferromagnetic state, and a large gap is opened up by the field. As a consequence, the susceptibility goes exponentially to zero as $T \to 0$. The double-peak merges into a round maximum, which decreases and shifts towards high temperatures with h ascending due to the enhancement of the gap as shown in Fig. 5(b).

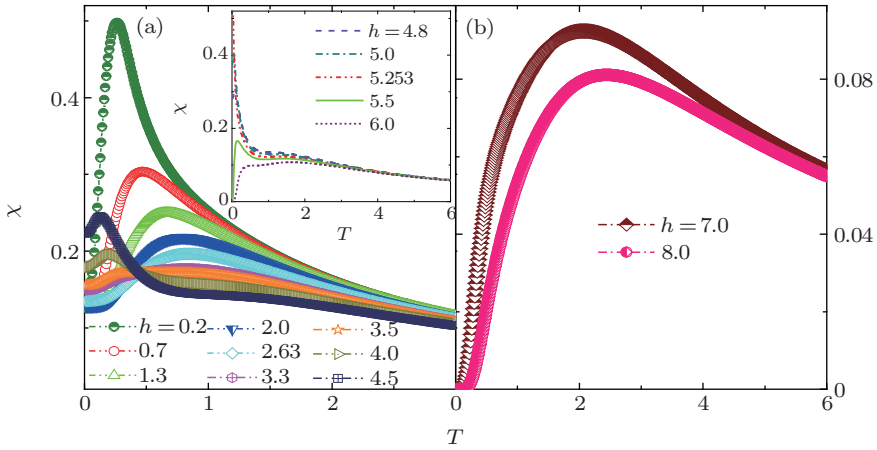


Fig. 5. (color online) Temperature dependences of the magnetic susceptibility for (a) $h < h_s$ and (b) $h > h_s$. The inset in panel (a) shows the curves of susceptibility versus temperature as h is close to h_s.

Figure 6 shows the temperature dependences of specific heat under different fields. In a weak field, the specific heat shows a double-peak structure due to the up-spin hole excitations of flat band, which is also observed in bipartite lozenge chain compounds $A_3Cu_3(PO_4)_4$ (A = Ca, Sr, and Pb)[49] as shown in Fig. 6(a). With the increasing of h, the flat band (up-spin) is pushed down deeply to the Fermi sea, resulting in the double-peak merging into a single one, which shifts towards the high temperature side. At ultra-low temperature, the variation of specific heat C_V/T with T displays a constant, i.e. C_V is T-varied linearly, indicating gapless behavior (see the inset).[46] As h approaches h_s, a shoulder emerges at low temperature, reflecting the important critical fluctuations. When h exceeds h_s but nearby, the low-temperature shoulder still exists, while as the field is higher and higher, the shoulder vanishes and only a single peak remains, which moves toward the high temperature side due to the larger gap opened up by the field, as shown in Fig. 6(b). However, at low temperature, the specific heat becomes exponentially activated (see the inset), where $\log(C_V)$ varies linearly with $1/T$, giving rise to $C_V \propto e^{-\Delta/k_B T}$. In fact, the slope of $\log(C_V)$–$1/T$ curve at low temperature manifests the magnitude of the energy gap $(-\Delta)$.[46] Apparently, for $h < h_s$ ($h = 2.0$ and 4.0), the slope of $\log(C_V)$–$1/T$ curve at low temperature is zero, suggesting the zero energy gap, of which the gapless behavior is in accordance with that in Fig. 6(a). In addition, at ultra-low temperatures, $C_V/T = 0$ (see the inset of Fig. 6(a)) because all spins are aligned along the field in the polarized ferromagnetic state, giving rise to the thermodynamic entropy remaining at a value of zero.

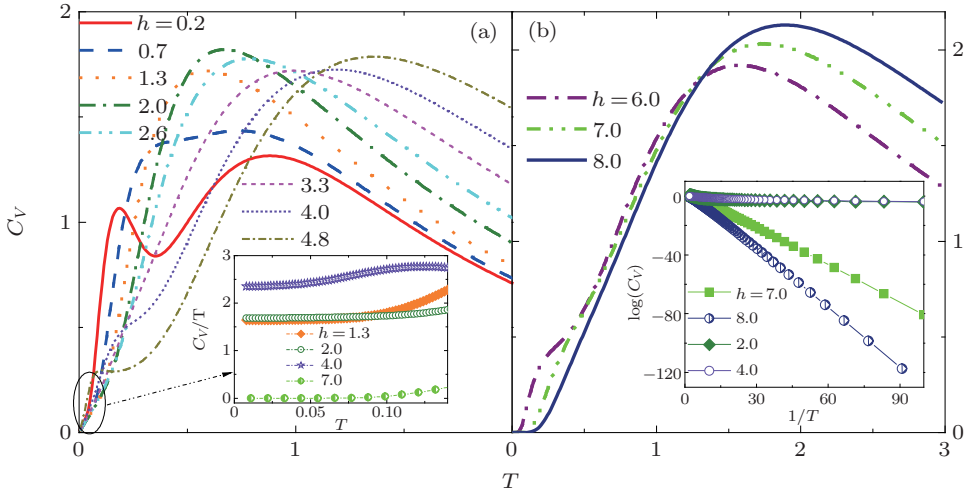


Fig. 6. (color online) Temperature dependences of the specific heat for (a) $h < h_s$ and (b) $h > h_s$; the inset of panel (a) shows the curves of C_V/T against T at ultra-low temperature; the logarithm of C_V as a function of $1/T$ is plotted in the inset of panel (b).

4. Conclusions

In this paper, we studied the magnetic properties and QPT of a bipartite lozenge periodic Anderson-like organic polymer by means of Green's function theory at half filling. The ground state of the system lies in gapless ferrimagnetism. At a finite temperature, a transition from a ferrimagnetic state to a paramagnetic phase occurs. The transition temperature can be reduced by Kondo screenings, while it can be enhanced by RKKY interaction, which stabilizes the magnetic order. Two Kondo screenings compete between each other, resulting in the localized f electron spin screened antiferromagnetically. Thus, in a magnetic field, it will make all spins align along the chain rapidly associated with a metal–insulator transition. Meanwhile, the single-site entanglement entropy can also be exploited as a useful tool to detect the QPT. In addition, we construct the temperature-field phase diagram, and reveal the gapless phase and spin polarized state, which are characterized by magnetic susceptibility and specific heat, denoting gapless or gapped low-lying excitation as a result of the competition between the up-spin and down-spin hole excitations.

References

[1] Korshak Y V, Medvedeva T V, Ovchinnikov A A and Spector V N 1987 *Nature* **326** 370
[2] Takahashi M, Turek P, Nakazawa Y, Tamura M, Nozawa K, Shiomi D, Ishikawa M and Kinoshita M 1991 *Phys. Rev. Lett.* **67** 746
[3] Macêdo A M S, Santos M C dos, Coutinho-Filho M D and Macêdo C A 1995 *Phys. Rev. Lett.* **74** 1851
[4] Raposo E P and Coutinho-Filho M D 1997 *Phys. Rev. Lett.* **78** 4853
[5] Xie S J, Zhao J Q, Wei J H, Wang S G, Mei L M and Han S H 2000 *Europhys. Lett.* **50** 635
[6] Zhao L, Yao K L and Duan Y F 2000 *Phys. Chem. Chem. Phys.* **2** 4001
[7] Wang W Z, Yao K L, Lin H Q and Li H T 1999 *Chin. Phys. Lett.* **16** 538
[8] Wang W Z and Yao K L 2002 *Chin. Phys. Lett.* **19** 262
[9] Wang W Z, Hu B B and Yao K L 2002 *Phys. Rev. B* **66** 085101
[10] Duan Y F, Yao K L and Yi L 2002 *Mod. Phys. Lett. B* **16** 179
[11] Montenegro-Filho R R and Coutinho-Filho M D 2005 *Physica A* **357** 173
[12] Wang W Z and Yao K L 2005 *Europhys. Lett.* **69** 978
[13] Guo J Y, Chen Y G and Chen H 2005 *Chin. Phys.* **14** 821
[14] Wang W Z 2006 *Phys. Rev. B* **73** 035118
[15] Stone M B, Broholm C, Reich D H, Tchernyshyov O, Vorderwisch P and Harrison N 2006 *Phys. Rev. Lett.* **96** 257203
[16] Yamamoto S and Ohara J 2007 *Phys. Rev. B* **76** 014409
[17] Fu H H, Yao K L and Liu Z L 2008 *J. Chem. Phys.* **128** 114705
[18] Coutinho-Filho M D, Montenegro-Filho R R, Raposo E P, Vitorianob C and Oliveirac M H 2008 *J. Braz. Chem. Soc.* **19** 232
[19] Gulácsi Z, Kampf A and Vollhardt D 2010 *Phys. Rev. Lett.* **105** 266403
[20] Sugano T, Blundell S J, Lancaster T, Pratt F L and Mori H 2010 *Phys. Rev. B* **82** 180401
[21] Jiang H, Hu G C and Xie S J 2010 *Physica B* **405** S299
[22] Suwa Y, Arita R, Kuroki K and Aoki H 2010 *Phys. Rev. B* **82** 235127
[23] Ding L J, Yao K L and Fu H H 2011 *Phys. Chem. Chem. Phys.* **13** 328
[24] Lopes A A and Dias R G 2011 *Phys. Rev. B* **84** 085124
[25] Hajj M A and Malrieu J P 2007 *J. Chem. Phys.* **127** 144902
[26] Shirakawa H, Louis E J, MacDiarmid A G, Chiang C K and Heeger A J 1977 *Chem. Commun.* 578
[27] Heeger A J 2001 *J. Phys. Chem. B* **105** 8475
[28] MacDiarmid A G 2001 *Angew. Chem. Int. Ed.* **40** 2581
[29] Dodabalapur A 2006 *Materialstoday* **9** 24
[30] Xiong Z H, Wu D, Vardeny Z V and Shi J 2004 *Nature* **427** 821
[31] Ovchinnikov A A 1978 *Theor. Chim. Acta* **47** 297
[32] Crommie M F 2005 *Science* **309** 1501
[33] Hooley C A and Mackenzie A P 2007 *Science* **317** 1332
[34] Gegenwart P, Si Q M and Steglich F 2008 *Nat. Phys.* **4** 186
[35] Tran M T and Kim K S 2011 *J. Phys.: Condens. Matter* **23** 425602
[36] Tsunetsugu H, Sigrist M and Ueda K 1997 *Rev. Mod. Phys.* **69** 809
[37] Gu S J, Tian G S and Lin H Q 2007 *Chin. Phys. Lett.* **24** 2737
[38] Zhu X and Tong P Q 2008 *Chin. Phys. B* **17** 1623
[39] Wang L C, Yan J Y and Yi X X 2010 *Chin. Phys. B* **19** 040512
[40] Fröbrich P and Kuntz P J 2006 *Phys. Rep.* **432** 223
[41] Ryndyk D A, Gutiérrez R, Song B and Cuniberti G 2009 *Energy Transfer Dynamics in Biomaterial Systems* (Berlin/Heidelberg: Springer) **93** 213
[42] Zimbovskaya N A 2008 *Phys. Rev. B* **78** 035331
[43] Gu S J, Deng S S, Li Y Q and Lin H Q 2004 *Phys. Rev. Lett.* **93** 086402
[44] Larsson D and Johannesson H 2006 *Phys. Rev. A* **73** 042320
[45] Maeda Y, Hotta C and Oshikawa M 2007 *Phys. Rev. Lett.* **99** 057205
[46] Hong T, Kim Y H, Hotta C, Takano Y, Tremelling G, Turnbull M M, Landee C P, Kang H J, Christensen N B, Lefmann K, Schmidt K P, Uhrig G S and Broholm C 2010 *Phys. Rev. Lett.* **105** 137207
[47] Gong S S, Gao S and Su G 2009 *Phys. Rev. B* **80** 014413
[48] Rost A W, Perry R S, Mercure J F, Mackenzie A P and Grigera S A 2009 *Science* **325** 1360
[49] Belika A A, Matsuo A, Azuma M, Kindo K and Takano M 2005 *J. Solid State Chem.* **178** 709